Taylor & Francis
Taylor & Francis Group

Journal of Electromagnetic Waves and Applications

ISSN: 0920-5071 (Print) 1569-3937 (Online) Journal homepage: www.tandfonline.com/journals/tewa20

Simulation and measurement methods of meander line antennas in human body conditions

Ngu War Hlaing, Kamilia Kamardin, Yoshihide Yamada, Angela Amphawan & Masaharu Takahashi

To cite this article: Ngu War Hlaing, Kamilia Kamardin, Yoshihide Yamada, Angela Amphawan & Masaharu Takahashi (04 Nov 2025): Simulation and measurement methods of meander line antennas in human body conditions, Journal of Electromagnetic Waves and Applications, DOI: 10.1080/09205071.2025.2582000

To link to this article: https://doi.org/10.1080/09205071.2025.2582000

JOURNAL OF ELECTROMAGNETIC WAVES AND APPLICATIONS
https://doi.org/10.1080/09205071.2025.2582000

Taylor & Francis
Taylor & Francis Group

Simulation and measurement methods of meander line antennas in human body conditions

Ngu War Hlaing[a], Kamilia Kamardin[b,c], Yoshihide Yamada[b], Angela Amphawan[a] and Masaharu Takahashi[d]

[a]School of Engineering and Technology, Sunway University, Subang Jaya, Malaysia; [b]Malaysia-Japan International Institute of Technology, Universiti Teknologi Malaysia, Kuala Lumpur, Malaysia; [c]Wireless Communication Center, Universiti Teknologi Malaysia, Kuala Lumpur, Malaysia; [d]Center for Frontier Medical Engineering, Chiba University, Chiba, Japan

ABSTRACT

A meander line antenna (MLA) is well known for its compact size and efficient performance in terms of antenna efficiency, input resistance, and bandwidth. This study investigates MLA performance in human body environments, focusing on medical devices and wireless implants. Due to their small size, MLAs are ideal for use in biological tissues with complex and lossy properties. The study analyzes MLA behavior in fat and muscle tissues, considering key parameters such as conductivity, radiation efficiency, and self-resonance. Input resistance and Voltage Standing Wave Ratio (VSWR) are examined. The smallest antenna size of $(14.9 \times 4.1 \times 0.1)$ mm³ is achieved. Human body phantoms for fat and muscle tissues were successfully formulated and fabricated, with dielectric constants aligning with reference values. A Q factor of approximately 2 was obtained through VSWR characteristics and validated against theoretical calculations, showing a 92% agreement. MLA gains of −30 dBi and −40 dBi were recorded in fat and muscle phantoms, respectively. These findings enhance the understanding of MLA performance in human tissue environments, supporting the development of next-generation implanted technologies for clinical and therapeutic applications.

ARTICLE HISTORY
Received 21 February 2025
Accepted 20 October 2025

KEYWORDS
Biomedical applications; fat; meander line antenna; muscle; radiation efficiency; self-resonance

1. Introduction

Innovative wireless communication systems that are integrated into the human body and enable an expanding range of wearable sensors, implants, and medical equipment are becoming more and more popular in biomedical engineering. These developments have the potential to improve patient quality of life, provide targeted medicines, and enable ongoing health monitoring, all of which require dependable, small, and effective antenna designs that can function well in intricate biological contexts [1]. Due to its small size and ability to achieve self-resonance at low frequencies, it is crucial for functioning in the extremely lossy environment of human tissue. The Meander Line Antenna (MLA) has become a very attractive alternative among the antenna designs being studied. The MLA's

CONTACT Ngu War Hlaing warhlaingn@sunway.edu.my School of Engineering and Technology, Sunway University, Subang Jaya, Selangor 47500, Malaysia

design, which is distinguished by a sinuous pattern that extends the current route within a compact form, is especially well-suited for applications in biomedical implants where there are substantial space constraints.

The performance of MLAs inserted in two different human tissue types, such as muscle and fat, is the focus of this investigation. The way electromagnetic waves travel through different tissues is influenced by their distinct conductive and dielectric characteristics [2]. Muscle tissue, for instance, is usually more conductive than fat, which results in higher rates of power loss and signal absorption [3]. This study intends to reveal the complex relationships between antenna design and biological tissue properties by methodically investigating the MLA's self-resonant conditions, radiation efficiency, and conductivity in these tissue environments. By supporting the optimization of MLA performance for biomedical applications, these insights aim to improve the functioning and dependability of implantable medical devices [4].

The MLA's capacity to achieve self-resonance under diverse tissue circumstances is one of the crucial elements examined in this study. Resonance is a crucial property of implanted antennas that affects radiation efficiency, signal transmission range, and clarity [5]. The dielectric characteristics of the surrounding tissues, in addition to elements such as antenna size, shape, and location within the body, must all be taken into consideration while designing MLAs [6]. Due to their distinct dielectric constants and conductivity levels, muscle and fat have various effects on the resonance of the MLA. Through the identification of configurations that enable the antenna to function at optimal efficiency in a variety of biological contexts, this work explores how the structural characteristics of the MLA can be adjusted to obtain optimal resonance in each kind of tissue [7]. It is anticipated that this research would help biomedical engineers improve MLA designs, allowing for better wireless communication and more effective energy use for bodily embedded devices.

To comprehend how well an antenna can carry power into human tissues, this study also focuses on radiation efficiency. Because of their high conductivity and permittivity, biological tissues with a high-water content, such as muscle, can drastically lower radiation efficiency by absorbing some of the power that the antenna transmits [8]. On the other hand, tissues like fat that contain less water might not affect signal attenuation as much, which could result in higher radiation efficiency. This study also looks at how tissue conductivity affects MLA performance. When determining how much of the transmitted electromagnetic energy is emitted as a useful signal and how much is wasted as heat within the tissue, conductivity is a crucial metric [9]. Because muscle and fat have varying conductivity levels, each type of tissue interacts with the MLA differently, which affects how well the antenna transmits signals overall [10].

To optimize signal transmission for MLAs in lossy environments, this study investigates the analysis of input resistance and its critical function. The dielectric characteristics of the surrounding tissues affect input resistance, which establishes impedance matching and reduces reflection losses for improved energy transfer [11]. To improve impedance matching across various tissue types, a comparative analysis of simulation and measurement findings reveals useful elements such as feeding cable effects. The study also examines the Voltage Standing Wave Ratio (VSWR) and its connection to the Q factor to enhance the MLA's bandwidth and operational stability and ensure dependable communication in implanted devices [12].

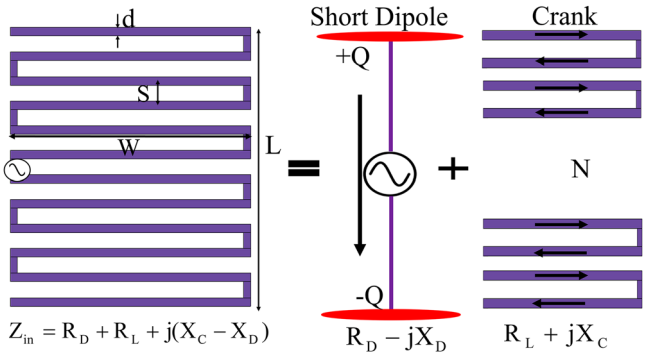

Figure 1. Equivalent current model of MLA [15].

This study contributes to the development of a thorough understanding of MLA functioning in human body situations. This study offers important new information for improving MLA designs utilized in biomedical engineering by examining conductivity interactions with human tissues, radiation efficiency, and self-resonant situations. The findings are intended to help guide and facilitate the development of more dependable, effective antennas that can function well in the wide range of human tissue compositions [13]. These advancements are anticipated to be crucial for the development of wireless medical devices, providing a route to next-generation implantable technologies that satisfy the exacting requirements of therapeutic and clinical applications.

To ensure biocompatibility for possible biomedical applications, the proposed MLA would be encapsulated with an appropriate covering material. Parylene-C, PDMS, and medical-grade silicone are common biocompatible coatings used in implantable devices [14]. These materials provide long-term tissue compatibility, avoid conductive element corrosion, and maintain structural stability without compromising the antenna's electromagnetic performance. Such encapsulation is consequently required for safe and dependable operation in implantable environments.

2. Methodology

2.1. Self-resonant conditions

The antenna structure of the meander line antenna is demonstrated with the current model shown in Figure 1 in which W is the antenna width, L is the antenna length, S is the spacing between each conductor, and d is the conductor width.

The expression for the input impedance (Z_{in}) is shown in Equation (1)

$$Z_{in} - R_D + R_L + j(X_C - X_D) \tag{1}$$

Here, X_D is the capacitive reactance of the short dipole antenna, and X_C is the inductive reactance of the bend line (crank). R_D and R_L are the radiation resistances of the short dipole and the conductive resistance of the antenna wire. X_C and X_D values can be canceled out by selecting suitable values for W, L, and N. Zero-reactance is known as the self-resonant condition and is essential for effective radiation generation. Equation (2) expresses the self-resonant condition. Figure 2 shows a Smith chart with a resonance point

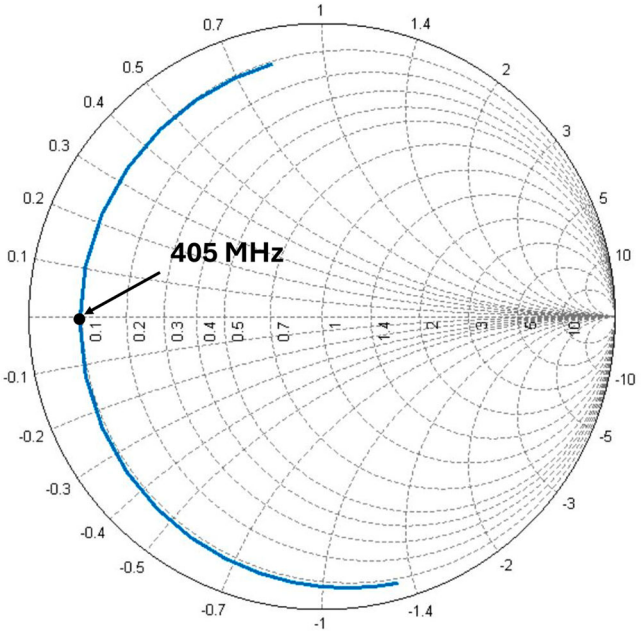

Figure 2. MLA self-resonance condition.

at 405 MHz noted in a black dot

$$R_{in} = R_D + R_L \tag{2}$$

It is anticipated that L (inductance) = 5nH, C (capacitance) would be 30.9 pF, and R would be 0.64 Ω If $f_0 = 405$ MHz, then $\omega_0 = 2\pi \cdot 405 \times 10^6$ rad/s and Q factor is 20, meaning the bandwidth BW = f_0/Q = 202.25 MHz.

To obtain the resonance point, the antenna width (W) is adjusted at fixed L and N, until the 405 MHz position is moved to $X = 0$. At this point, set W is said to be the antenna's resonant width. By repeating the process for different L and N conditions, a self-resonant structure curve is obtained.

2.2. Self-resonant conditions in muscle

The self-resonant conditions of MLA in human body parts, such as muscle and fat, are simulated, and the self-resonant structures are obtained from the electromagnetic simulation results. The antenna input impedances, surface current distributions, and VSWR are observed in this section.

The starting geometry of the structure is defined by the normalized length ratio (L/λ_g) and the number of turns (N), which are chosen at the start of the design process. The physical arrangement is established by calculating the conductor width (d) and spacing (S) based on these characteristics. The target resonance frequency of 405 MHz is then attained by iteratively adjusting the conductor width (W) [15]. Lastly, the structure is adjusted to retain fabrication feasibility and guarantee correct 50 Ω impedance matching.

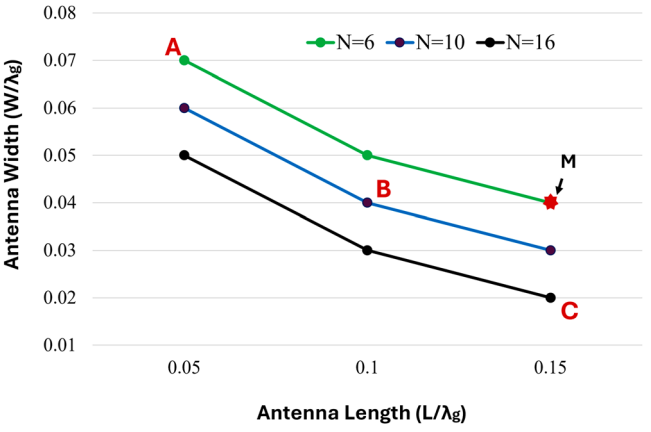

Figure 3. Self-resonant structures of MLA in muscle.

Table 1. Comparison of the resistance simulation and theoretical results.

		R_{in} (σ_C) (Ω)		R_{in} (∞) = R_D (Ω)		R_L (Ω)				η (dB)	
Body	Type	Sim	Equation (3)	Sim	Equation (6)	Sim	Equation (5)	R_{abs} (Ω)	R_{in} (σ = 0) (Ω)	Sim	Equation (5)
Mus	A	30.9	31.38	0.007	0.01	2.63	3.12	28.25	2.648	−36	−35
	B	35.3	35.82	0.014	0.026	2.81	3.31	32.48	2.819	−34	−31
	C	41	41.61	0.031	0.037	3.51	4.11	37.46	3.541	−31	−30
Fat	A	41.8	42.24	0.024	0.023	1.34	1.82	40.44	1.44	−32	−32
	B	50	50.66	0.048	0.056	1.38	2.14	48.47	1.53	−30	−29.5
	C	53.4	54.23	0.081	0.079	1.52	2.35	51.8	1.6	−28.2	−28.3

The simulation results of antenna widths of self-resonant structure for N = 6, 10, and 16 with L/λ_g = 0.05, 0.1, and 0.15 in muscle conditions are shown in Figure 3.

The antenna spacing was calculated by using S = L/(2N−1). The conductor width (d) was selected as 0.1 mm for N = 6 and 10, but 0.08 mm for N = 16, since the spacing at N = 16 is extremely small. The red star indicates the spacing is very small, which is 0.16 mm; thus, d = 0.1 mm is impossible to set up. To analyze with the same width at the same number of turns (N), for N = 16, d is chosen to be 0.08 mm for all three structures. The antenna width is adjusted until the self-resonant condition is obtained. The antenna input resistance is recorded. The wavelength of MLA in muscle conditions is 98 mm. For comparison of antenna different structures, structures A (N = 6, L/λ_g = 0.05), B (N = 10, L/λ_g = 0.1), and C (N = 16, L/λ_g = 0.15) are selected as shown in Table 1. For fabrication, N = 6, L/λ_g = 0.15, and d = 0.1 mm were selected because this structure is convenient for fabrication, and the input resistance is large enough for impedance matching with 50 Ω coaxial cables.

The self-resonant structures of the antenna with (W/λ_g) versus antenna length (L/λ_g) are plotted in Figure 3. The antenna structure for fabrication is pointed "M." From the results, it can be observed that if the antenna length becomes longer, the antenna width becomes smaller. As for N dependence, the antenna width (W) decreased with the increase of N. The antenna input resistance of structures A, B, and C is shown in Figure 4. It can

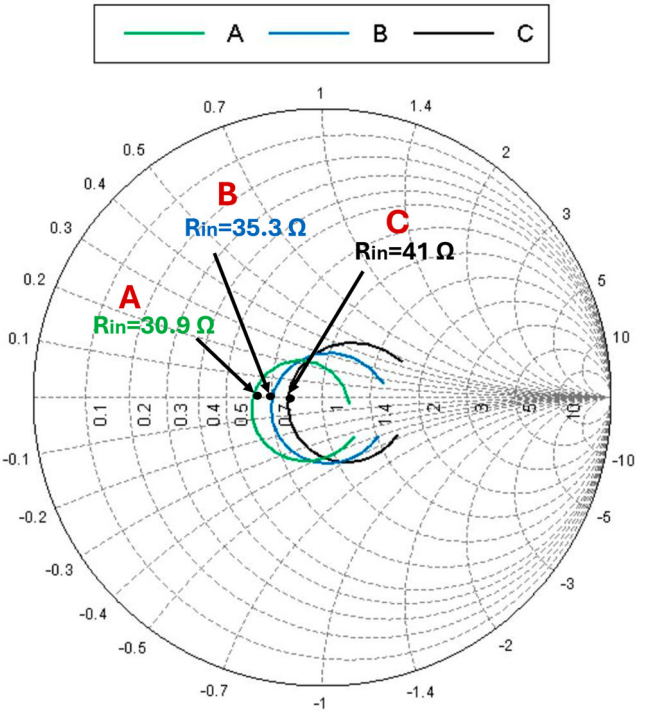

Figure 4. Antenna input resistances of Structures A, B, and C.

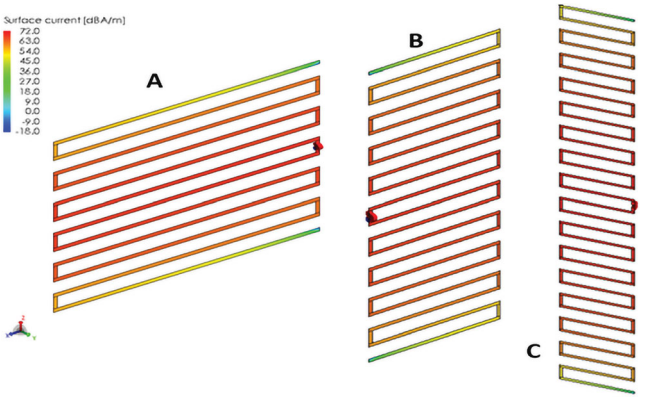

Figure 5. Current distribution of structures A, B, and C in the muscle.

be observed that with the longer antenna length, structure C has wider Smith chart characteristics compared to structures A and B. The larger the antenna length, the larger the antenna input resistance can be obtained.

Figure 5 shows the antenna current distribution of structures A, B, and C in muscle conditions. They are uniformly distributed, and the maximum current occurs at the feeding line. According to Figure 6, when the number of turns (N) and antenna lengths increase, the input resistance (Rin) also increases.

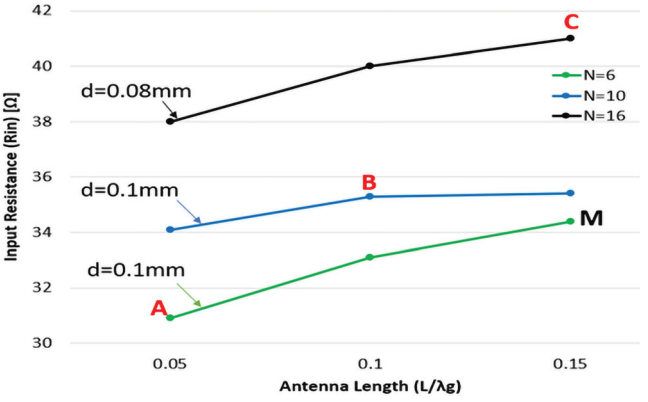

Figure 6. Antenna input resistances of structures A, B, and C.

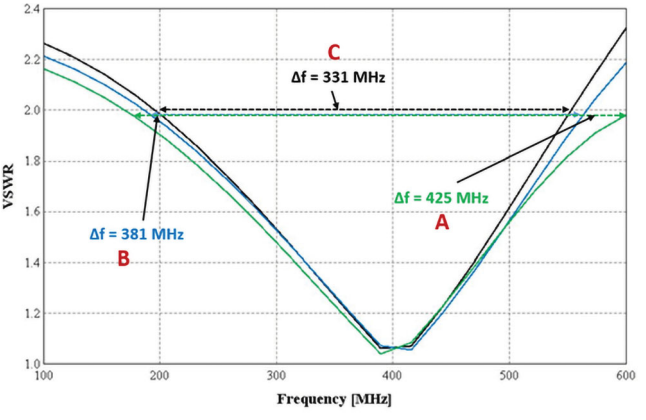

Figure 7. VSWR of structures A, B, and C in the muscle.

The simulation results of VSWR characteristics are compared in Figure 7.

As seen in Figure 7, the wider bandwidth occurs at structure A compared to structures B and C. It means the smaller length of the antenna has the higher bandwidth. The bandwidth percent of simulations of structures A, B, and C is 105 percent, 94 percent, and 82 percent, respectively.

2.3. Self-resonant conditions in fat

The simulation results of antenna widths of self-resonant structure for N = 6, 10, and 16 with $L/\lambda_g = 0.05$, 0.1, and 0.15 in fat conditions are shown in Figure 8. The conductor width (d) was selected for 0.5 mm for N = 6, 10, and 16 because the antenna lengths and spacing are quite large compared to the structures of MLA in muscle and conditions. Moreover, different values of conductor width do not affect the structures of self-resonance, but affect Rin values.

For fabrication, N = 6, $L/\lambda g = 0.1$, and d = 0.5 mm were selected because this structure is convenient for fabrication, and the input resistance is large enough for impedance

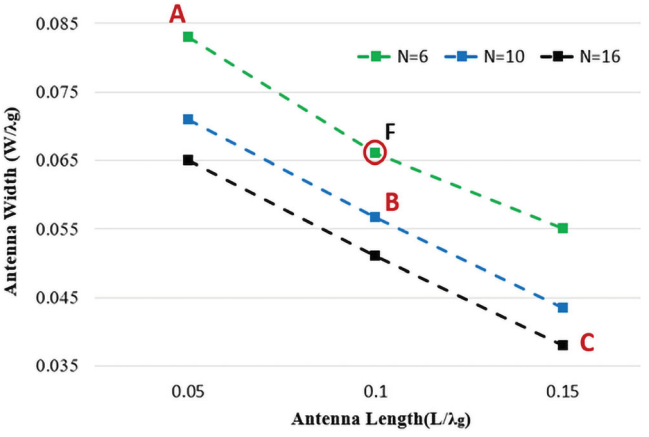

Figure 8. Self-resonant structures of MLA in fat tissue.

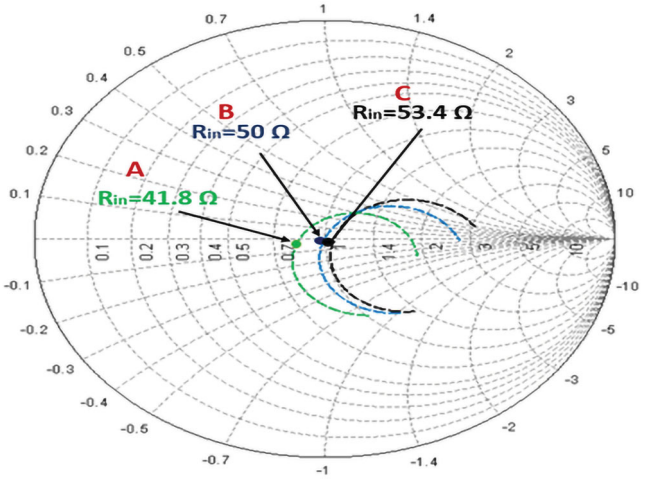

Figure 9. Antenna input resistances of structures A, B, and C in fat tissue.

matching with 50 Ω coaxial cable. Point "F" indicates the structure for fabrication. The self-resonant structures of the antenna with (W/λg) versus antenna length (L/λg) are plotted in Figure 8. From the results, it can be observed that if the antenna length becomes longer, the antenna width becomes smaller. As for N dependence, the antenna width (W) decreased with the increase of N.

The antenna input resistance of structures A, B, and C is shown in Figure 9. In a similar manner to the MLA of muscle conditions, the MLA in fat condition shows that the longer antenna length, structure C has wider Smith chart characteristics compared to structures A and B. The larger the antenna length, the larger the antenna input resistance.

Figure 10 shows the antenna current distribution of structures A, B, and C in fat conditions. Similarly, with muscle conditions, they are uniformly distributed, and the maximum current occurs at the feeding line. The input resistances of the self-resonant structure graph are shown in Figure 11. Similar to MLA in muscle conditions, when the number of turns

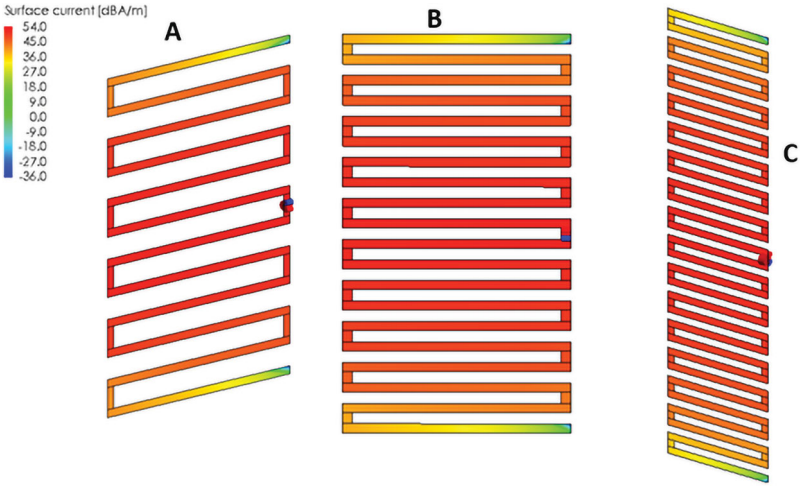

Figure 10. Current distribution of structures A, B, and C in fat.

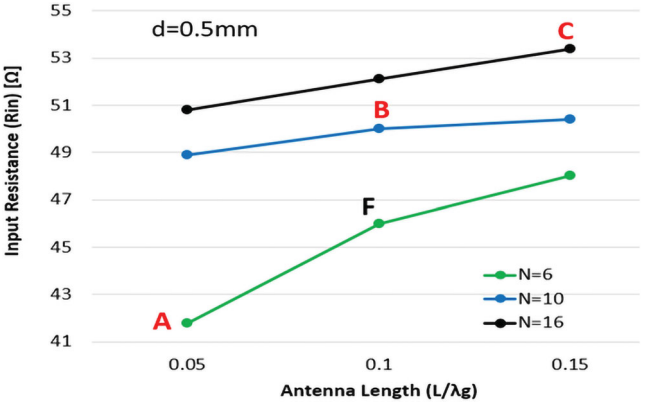

Figure 11. Input resistances of structures A, B, and C in fat.

(N) and antenna lengths increased, the input resistance (Rin) also increased. The simulation results of VSWR characteristics are compared in Figure 12. As seen in Figure 10, the wider bandwidth occurs at structure A compared to structures B and C.

It means the smaller length of the antenna has a higher bandwidth. The bandwidth percent of simulations of structures A, B, and C is 50.8 percent, 46.7 percent, and 43.9 percent, respectively.

2.4. Analysis of radiation efficiency of MLA in muscle and fat tissues

To validate the correctness of simulation results, the theoretical results of antenna resistances are compared with the simulation results. The antenna input resistance (R_{in}) can be obtained by the addition of antenna radiation resistance (R_D), conductive resistance (R_L),

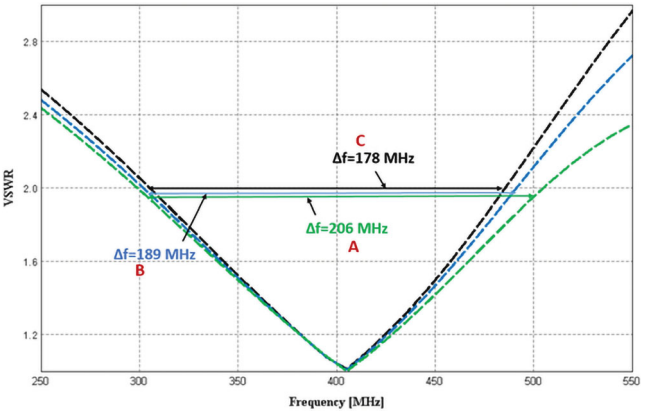

Figure 12. VSWR of structures A, B, and C in fat.

and absorptive resistance (R_{abs}) as expressed in Equation (3)

$$R_{in} = R_D + R_L + R_{abs} \tag{3}$$

R_{abs} can be obtained by subtracting the antenna input resistance with antenna wire conductivity $\sigma_c = 0$ S/m from the antenna input resistance with $\sigma_c = 5.86 \times 107$ S/m. To obtain the R_D in the simulation, the PEC ($\sigma_c = \infty$) condition is applied to the antenna wire

$$R_{abs} = R_{in(\sigma)} - R_{in(\sigma=0)} \tag{4}$$

where the initial assumption is that the absorbed resistance, R_{abs}, is a function strongly dependent on the σ value.

Figure 13 shows the input resistance R_{in} versus L/λ_g of $\sigma = 0.79$ and 1.2 (S/m). For $\sigma = 0$ (S/m), human tissues are considered a lossless medium, and the R_{abs} component is equal to zero, R_{abs} ($\sigma = 0$). For the case of a lossy medium where $\sigma \neq 0$ (S/m), R_{abs} is added to the existing input resistance; hence, R_{in} becomes much larger. To clarify the situation, a graph of input resistance versus conductivity for structure point A is plotted in Figure 13. It is shown that the R_{abs} significantly contributes to R_{in} and increase proportionally with conductivity. R_{in} increases rapidly from 2.639 Ω ($\sigma = 0$) to 24.67 Ω ($\sigma = 0.4$) before becoming saturated from that point onward until $R_{in} = 30.889$ Ω ($\sigma = 0.79$), and not much change is observed. Next, the relation between different σ and ϵr is presented in Figure 14.

From the derivation of conductive resistance and radiation resistance for human body conditions, the conductive resistance (R_L) and radiation resistance (R_D) are expressed in Equations (5) and (6), respectively

$$\mathrm{R}_L - 2\pi \times \frac{2NW + L}{2(d+t)} \sqrt{\frac{30}{\sigma_c \lambda_g}} \tag{5}$$

$$\mathrm{R_D} - \sqrt{\frac{\mu_r}{\varepsilon_r}} 20\pi^2 (\mathrm{L}/\lambda_g)^2 \tag{6}$$

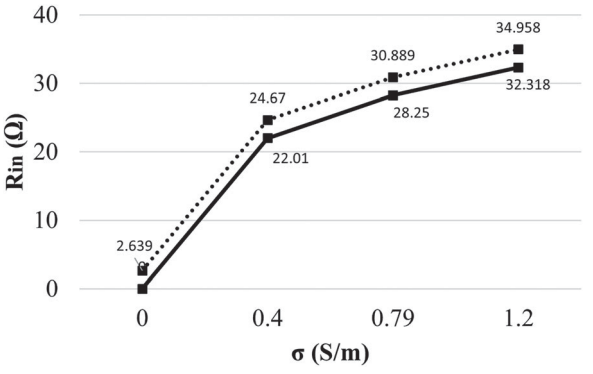

Figure 13. Resistances of the structure at structure A in the muscle.

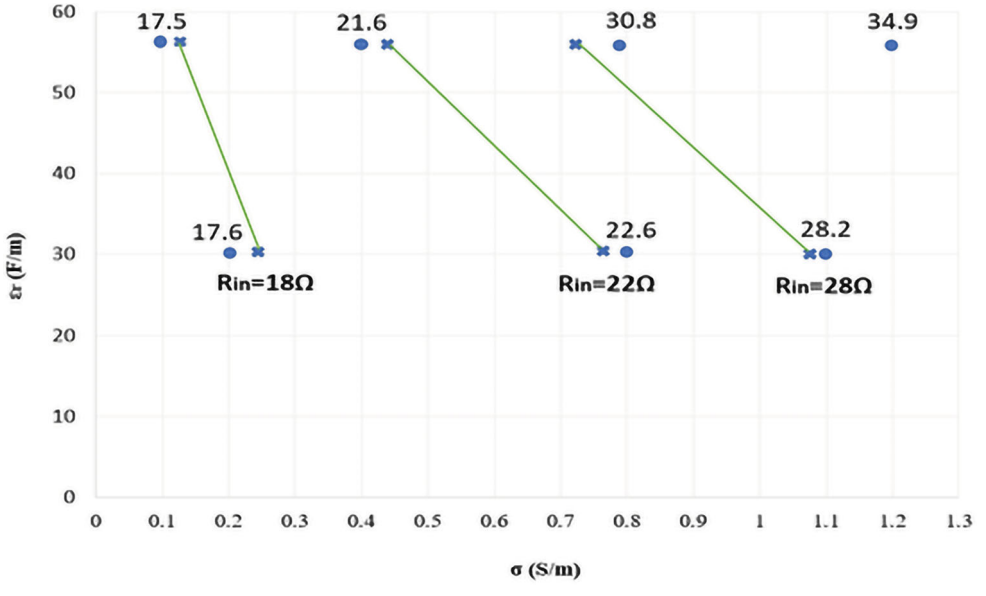

Figure 14. Permittivity relation with conductivity.

To observe the antenna efficiency (η), Equation (7) can be applied

$$\eta = 10\log\left(\frac{R_D}{R_{in}}\right) dB \tag{7}$$

First, the simulation results of R_{in} ($\sigma_c = 0$) and R_D ($\sigma_c = \infty$) of MLA of structures A, B, and C in muscle and fat conditions are shown in Figures 15 and 16.

As can be seen in Figures 15 and 16, R_{in} ($\sigma_c = 0$) and R_D ($\sigma_c = \infty$) in muscle and fat conditions gradually increase if the antenna structure becomes larger, which is in a similar manner to R_{in}.

The theoretical results of input resistances, conductive resistances, and radiation resistances are compared with the simulation results in Table 1. They show that they have a good

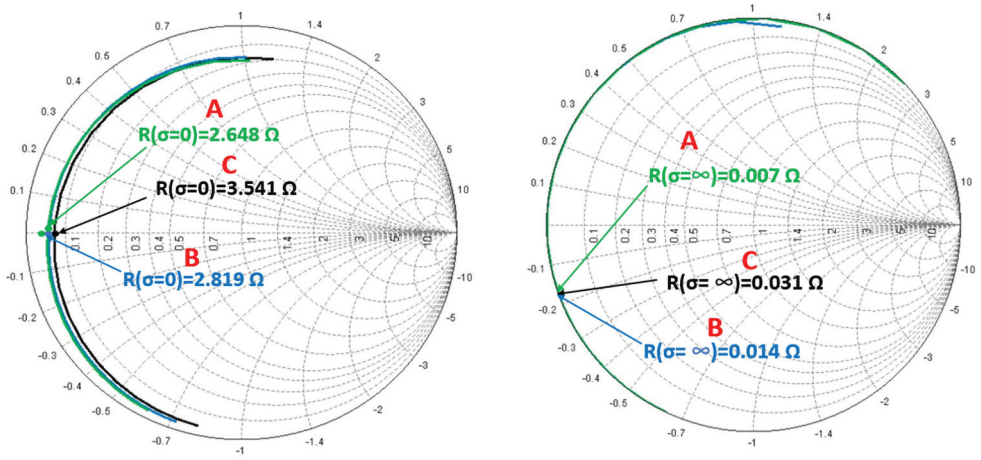

(a) R_{in} (σ_c=0) (b) R_D (σ_c=∞)

Figure 15. R_{in} ($\sigma_c = 0$) and RD ($\sigma_c = \infty$) in muscle conditions.

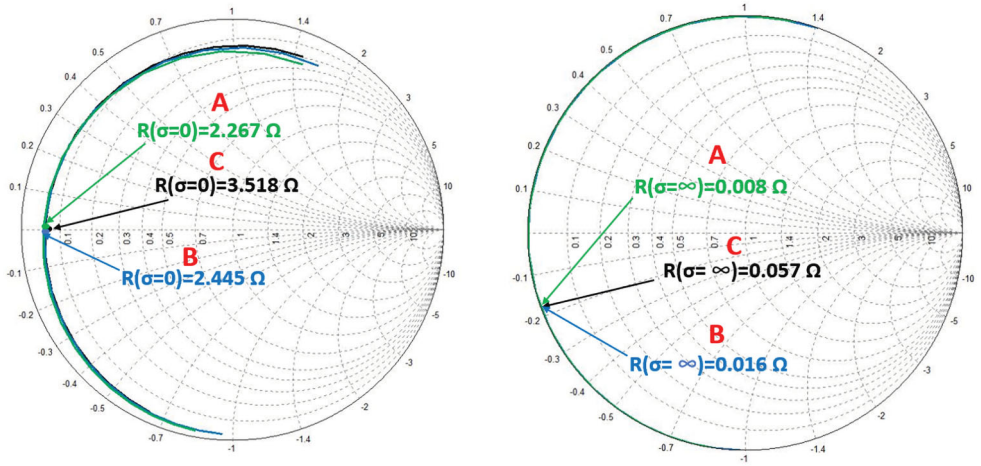

(a) R_{in} (σ_c=0) (b) R_D (σ_c=∞)

Figure 16. Rin ($\sigma c = 0$) and RD ($\sigma c = \infty$) in fat conditions.

agreement. Absorptive resistance is calculated based on Equation (4). The efficiency is calculated and compared with the simulation results, and they also have a good agreement. Thus, the simulation results are accurate and validated.

For the lower permittivity value of the fat condition, a larger input resistance is obtained compared to the higher permittivity values of the muscle condition. Moreover, the larger structure C has a higher input resistance value compared to the smaller structures A and B. Furthermore, all the structures have good agreement in simulation and theoretical results. For higher conductivity of muscle condition, the higher conductive resistance occurs compared to lower conductivity values in fat condition [12]. The larger antenna structure C has a higher conductive resistance compared to the smaller structures A and B.

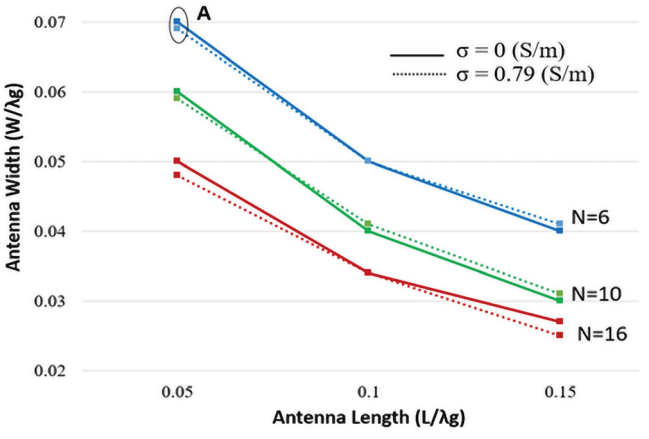

Figure 17. Self-resonant structures of MLA in muscle conditions with different conductivities.

Despite having a maximum 0.7 Ω difference between simulation and theory, the R_L of structures A, B, and C all exhibit the same tendency. Higher efficiency occurs in lower conductivity and permittivity values of fat conditions compared to higher conductivity and permittivity of muscle conditions. The simulation and theoretical results have good agreement.

2.5. Conductivity analysis of MLA in human body conditions

The procedure to obtain self-resonant structures has already been explained in this section. Figure 17 shows the self-resonant structures of MLA in human muscle equivalent medium when $\epsilon_r = 57$ for two conductivity values, $\sigma = 0$ (S/m) and $\sigma = 0.79$ (S/m). Figure 16 shows the self-resonant structures of MLA in the human fat equivalent medium when $\epsilon_r = 12.21$ for two conductivity values, $\sigma = 0$ (S/m) and $\sigma = 0.119$ (S/m). The lower conductivity value is set to see the effect of conductivity on the resonant structure of the antenna [16]. Here, the width of the antenna, W, and length, L, are normalized with the wavelength of the material, λ_g.

Figure 17 shows no significant difference in the resonant curve for different values of σ. Thus, it can be considered that conductivity does not change the dimensions of MLA in terms of W and L. Therefore, the conductivity of human body tissues is considered not to affect the resonant condition of MLA [17].

In Figure 18, it can be seen that W becomes smaller with an increasing number of turns, N. The results agree with a previous study [18]. This is because W and N strongly depend on capacitive reactance (X_D) and inductive reactance (X_C). With increasing N, the dimension of the antenna is also effectively reduced. This is an essential factor for an antenna in the human body, since the miniaturization of the antenna is one of the requirements. The antenna structure at point A is selected to check the antenna resistance changes when different conductivity values are set.

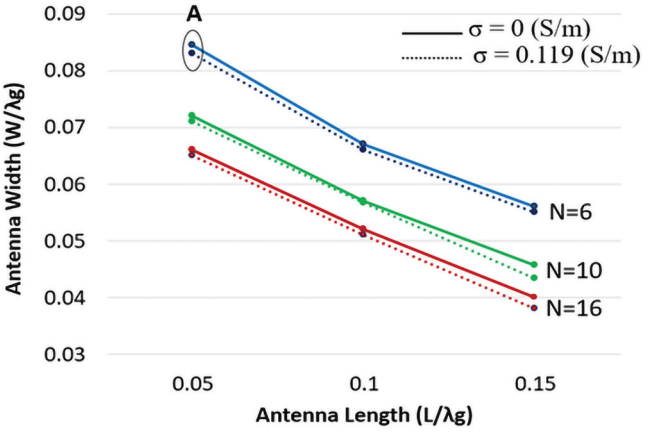

Figure 18. Self-resonant structures of MLA in fat condition with different conductivities.

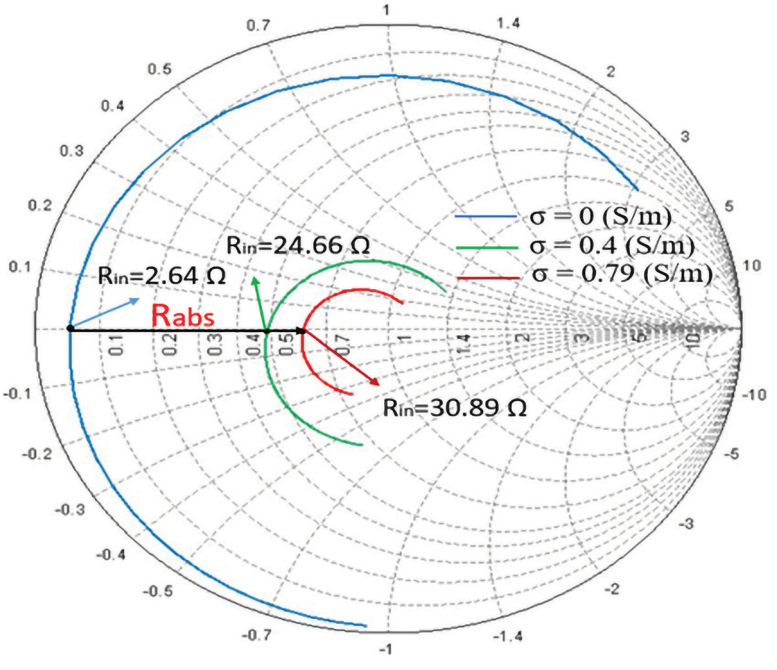

Figure 19. Input impedance of structure A in Muscle conditions with different conductivity values.

2.6. Antenna input resistance analysis of MLA in human body conditions

The simulation results of input resistance are shown in Figure 19 to be $R_{in} = 30.89\,\Omega$, $R_{in} = 24.66\,\Omega$, and $R_{in} = 2.64\,\Omega$ at $\sigma = 0.79$ S/m, 0.4 S/m, and 0 S/m, respectively. The input resistance for $\sigma = 0.79$ is more significant than for $\sigma = 0.4$. For a lossless medium, R_{in} at $\sigma = 0$ S/m is shown to be very small, less than $2\,\Omega$.

Due to the high conductivity, most resistance components are due to absorption by a dielectric material. The resistance loss by the absorbance of the phantom is denoted by R_{abs} (previously R_{loss}). The input resistance inside the phantom is very high compared to

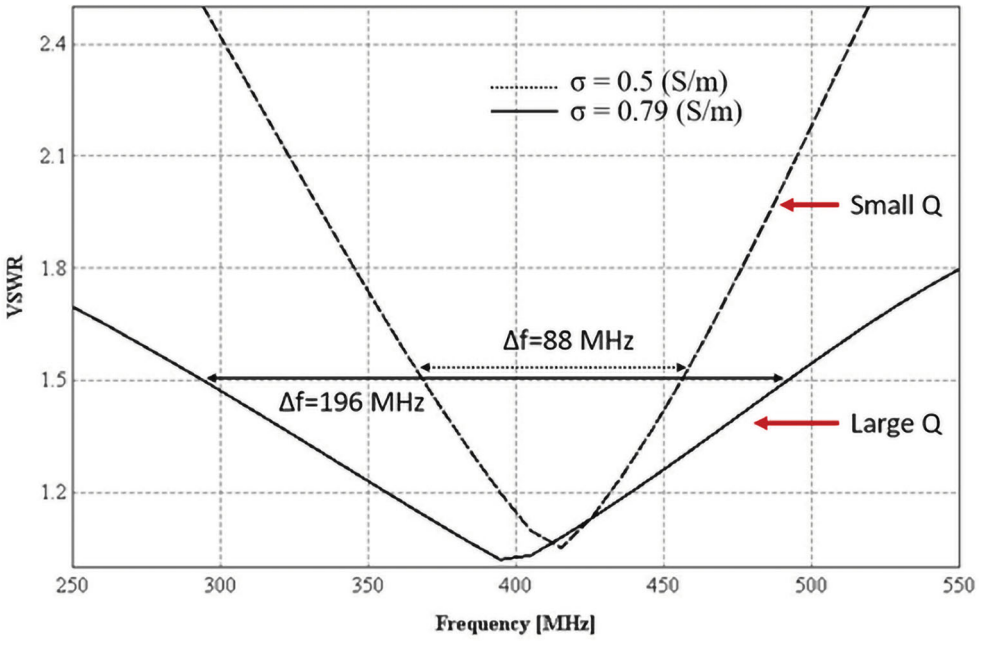

Figure 20. BW of MLA for different σ.

the antenna in free space because of the dielectric material surrounding it [19]. The initial assumption is that R_{abs} largely depends on the conductivity, σ, value.

2.7. Antenna bandwidths analysis of MLA in human body conditions

A smaller MLA structure, point A with dimensions given by (4.9 × 6.8) mm^2 (L × W), was simulated to investigate the effect of conductivity on the antenna bandwidth. The simulation results are shown in Figure 20. MLA bandwidth for $\sigma = 0$ (S/m) is indicated by dotted lines, while the solid lines for the bandwidth for $\sigma = 0.79$ (S/m). The bandwidth can be calculated as Equation (8)

$$BW = \frac{\Delta f}{f}. \tag{8}$$

The obtained BW for $\sigma = 0.5$ is 21.7 percent, and for $\sigma = 0.79$ is 48 percent. Thus, Q_{eq} for $\sigma = 0.5$ is 1.88, and for $\sigma = 0.79$ is 0.85. Therefore, a smaller conductivity value gives a larger Q. In the previous section of the antenna input resistance analysis, it can be seen that R_{in} increases with higher σ. Thus, it is concluded that a wider bandwidth will be achieved with higher conductivity.

2.8. Phantoms fabrication

The suitable size of the phantom is 80 mm in length, and 70 mm for cylindrical diameter. The volume is (80 × 70 × 70) mm^3. The recipe to make fat and muscle phantoms at

Table 2. Recipes for phantoms.

Chemical	Fat	Muscle
Distilled water (ml)	–	420
Glycerin (ml)	400	–
Polyethylene powder (g)	220	56
Agar (g)	16	20
Xanthan gum (g)	16	16
Sodium chloride (g)	–	1.4
Sodium dehydroacetate monohydrate (g)	–	0.26

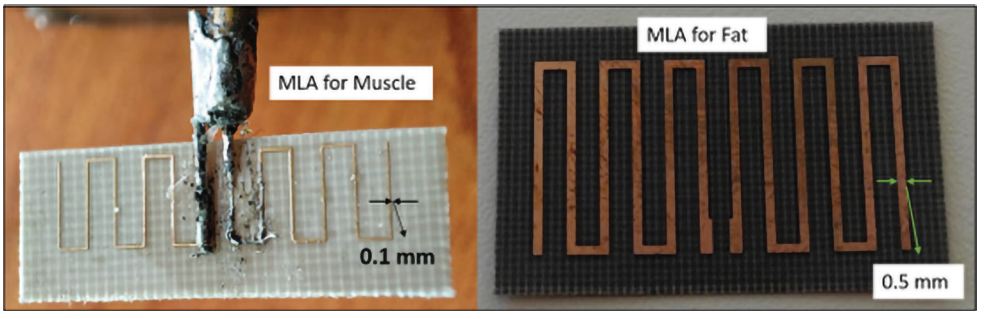

Figure 21. Fabricated Implantable antennas.

405 MHz is shown in Table 2. Here, the individual effect of each material is also stated [20].

For agar powder, it is used to gather all the ingredients to form a fat phantom in a liquid–solid state [21]. The xanthan gum is applied as a thickener to increase the phantom's stickiness. Sodium dehydroacetate is a preservative that prevents the phantom from degrading fast, particularly from fungus. It is very important to take great care of mixing sodium chloride, as it directly affects the phantom's relative conductivity. Since fat tissue has a low conductivity value ($\sigma = 0.119$ S/m), sodium chloride is unnecessary. But for the high conductivity of muscle ($\sigma = 0.79$ S/m), sodium chloride plays a major role in obtaining the correct conductivity value.

2.9. Antennas fabrication

MLA structures with $N = 6$, $L/\lambda_g = 0.1$, $L = 21.2$ mm, and $W = 15$ mm (structure F) for fat tissue, and $N = 6$, $L/\lambda_g = 0.15$, $L = 14.9$ mm, and $W = 4.1$ mm (Structure M), were fabricated as shown in Figure 21.

To place the MLA between the fat and muscle phantoms for measurement, shallow pits of suitable size are made on the surface of the phantoms. Then, the antenna is embedded inside the phantoms as shown in Figure 22.

The target values of conductivity and permittivity of fat and muscle phantom are almost the same as listed in Table 3.

For the radiation pattern, the antenna was set up inside an anechoic chamber. A half-wavelength dipole antenna was used as the gain reference antenna. The log-periodic

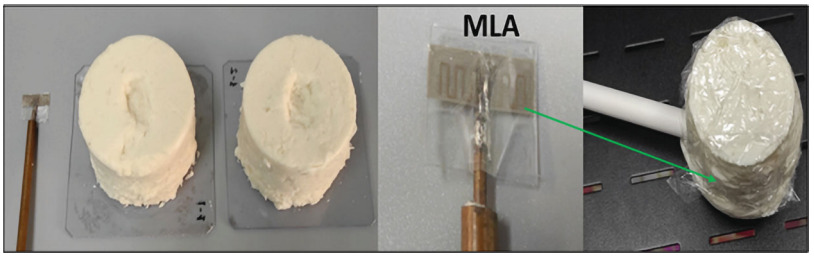

Figure 22. Antennas embedded in phantoms.

Table 3. Target and fabricated dielectric values.

	Fat	Muscle
Target	$\sigma = 0.119$ S/m	$\sigma = 0.79$ S/m
	$\epsilon_r = 12.21$ F/m	$\epsilon_r = 57$ F/m
Fabricated	$\sigma = 0.13$ S/m	$\sigma = 0.715$ S/m
	$\epsilon_r = 11$ F/m	$\epsilon_r = 56.2$ F/m

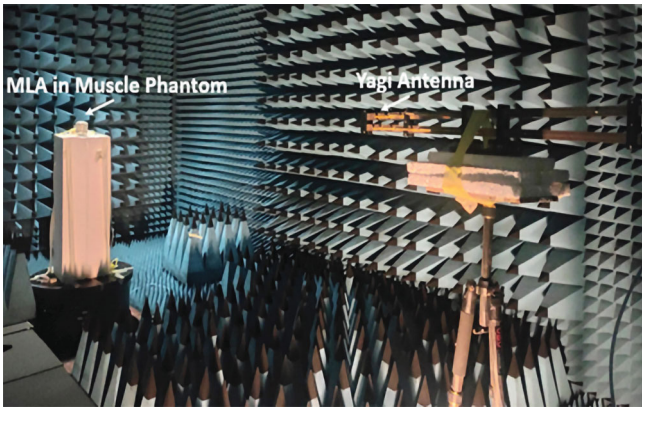

Figure 23. Set up for radiation pattern measurement.

antenna was placed on the tripod as a transmit antenna. The radiation pattern measurement setup is shown in Figure 23. The MLA inside the fat and muscle phantom was set to be the receiver (Rx), and the Yagi antenna was set to be the transmitting antenna (Tx).

3. Results and discussion

3.1. Measurement of input resistance in fat tissue

Input resistance at the resonant point of structure F with a dimension of 21.2 × 15 mm (L × W) and N = 6 was measured inside the fabricated phantom. The dielectric constant of the fat phantom is $\epsilon_r = 11$ (F/m) and $\sigma = 0.13$ (S/m). The simulated and measured results of the input resistance (R_{in}) are presented in Figure 24. The solid curve is the measured result, while the dotted curve indicates the simulation result.

From the simulation, the input resistance at 405 MHz is given as R_{in} (sim) = 48.9 Ω, while the measured value is obtained as R_{in} (meas) = 46.72 Ω. The measured results

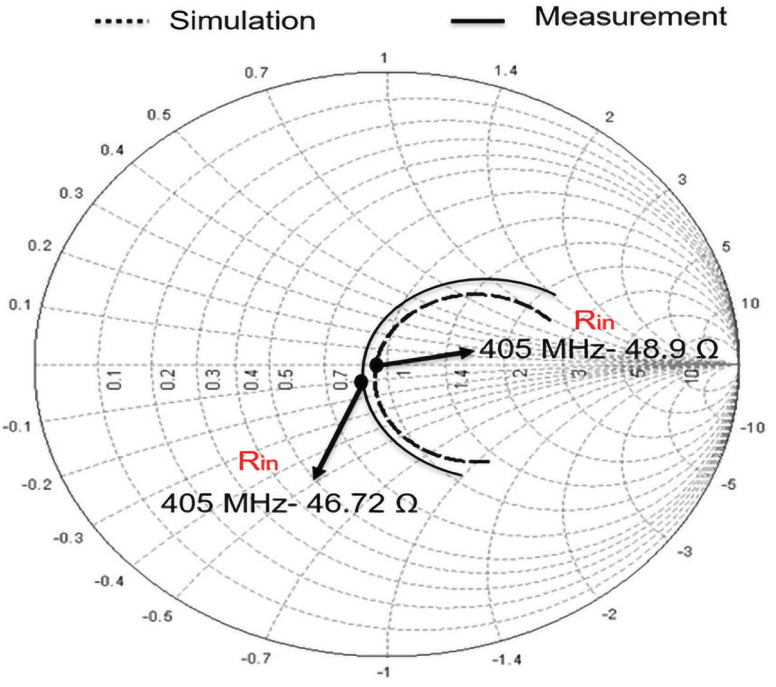

Figure 24. Input resistances of measured and simulated MLA in fat tissue.

decreased from the simulation results by 2.18 Ω. However, this decrease might be attributed to the effect of feeding cables.

3.2. Antenna Q factor in fat tissue

The simulated and measured results of the VSWR are presented in Figure 25. The solid curve is the measured result, while the dotted curve indicates the simulation result. From the simulation, the frequency range at VSWR = 2 at 405 MHz is given as Δf (sim) = 160 MHz, while the measured value is obtained as Δf(meas) = 140 MHz.

The measured results decreased from the simulation results by 20 MHz. It can be because of the feeding cables. The waveform and the frequency of the measurement result are slightly shifted to the right compared to the simulation results. The bandwidth of the simulation is 39 percent, and the measurement is 34 percent, respectively.

As shown in Figure 25, the VSWR values of the measurement and simulation results of structure F have a good agreement. The Q factor is closely related to bandwidth (BW). The Q factor of VSWR can be obtained from Equation (9)

$$Q_{VSWR} = \frac{VSWR - 1}{BW\sqrt{VSWR}} \tag{9}$$

Since VSWR = 2, then, Q of bandwidth is given as follows:

$$Q_{VSWR} = \frac{1}{BW} \times \frac{1}{\sqrt{2}} = \frac{f_0}{\Delta f} \times \frac{1}{\sqrt{2}} \tag{10}$$

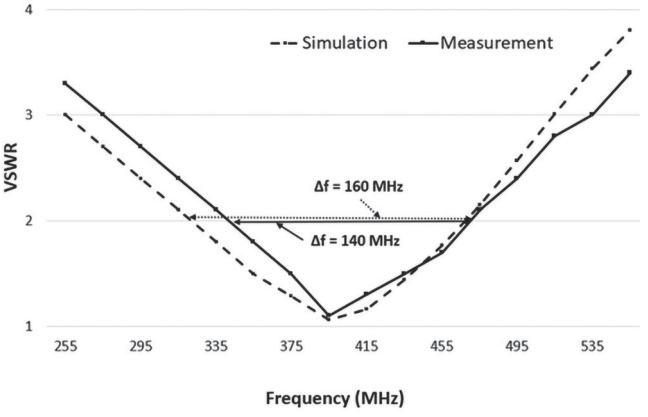

Figure 25. Input resistances of measured and simulated MLA in fat tissue.

Table 4. Calculated values of Qeq and QVSWR.

Structure F	X_C (Ω)	R_{in} (Ω)	Δf (MHz)	Q_{eq}	Q_{VSWR}
Simulation	115.25	48.9	160	2.35	1.8
Measurement		46.72	140	2.46	2.1

The Q factor can also be calculated by the ratio of reactance to the input resistance (R_{in})

$$Q_{eq} = \frac{X_C}{R_{in}} \tag{11}$$

The proposed inductive reactance (X_C) equation is expressed in Equation (12), where $W/\lambda g = 0.066$, $L/\lambda g = 0.1$, $N = 6$, and $d = 0.5$ mm for structure F. According to Table 4, the Q factors obtained from Equations (9) and (10) are compared based on the simulation and measurement results. The simulation result of Q_{eq} is 2.35, and the simulation result of Q_{VSWR} is 1.8. In measurement, Q_{eq} is 2.46, and the Q_{VSWR} is 2.1. Moreover, simulation results and measured results of the Q factor have a good agreement. As a result, the simulation and equation results can be assumed to be consistent

$$X_C = \frac{240\pi N}{\sqrt{\varepsilon_r}} \times \frac{W}{\lambda_g} ln \frac{\frac{L}{\lambda_g}}{\frac{d}{\lambda_g}(2N-1)} [\Omega] \tag{12}$$

3.3. Measurement of antenna gain in fat tissues

The simulation results of three-dimensional (3D) radiation patterns of structure F are shown in Figure 26. The total realized gains of structure F are −30 dBi. The peak radiation direction appeared in the horizontal direction.

The radiation pattern measurement comparisons of structure F to a half-wave dipole are shown in Figure 22. In Figure 22, ΔG indicates the gain reduction of the half-wave dipole antenna. It means the gain difference between the MLA and the half-wavelength dipole. For structure F, ΔG1 and ΔG2 are −30.32 dB and −30.81 dB, respectively. To obtain the

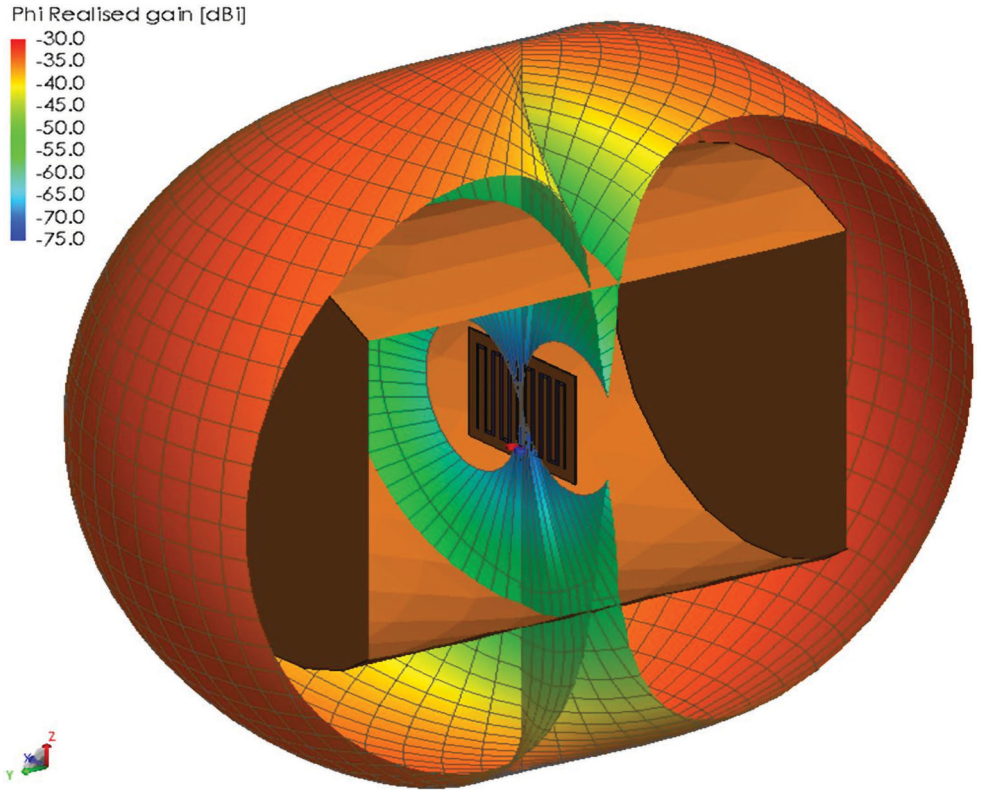

Figure 26. The three-dimensional radiation pattern of MLA in fat.

correct antenna gain measurement results, many different settings of dipole antenna position were investigated, and the average values of dipole radiation patterns were taken to estimate the correct results of ΔG values. The calculated value of the antenna gain (G_{cal}) can be estimated using Equation (13) (Figure 27)

$$\Delta G = \frac{\Delta G_1 + \Delta G_2}{2} = -30.565 dB \tag{13}$$

Then, the measurement result of antenna gain can be calculated using Equation (14)

$$G_{meas} = \Delta G + 2.15 = -28.42 dBi \tag{14}$$

The estimated gain can be obtained by using Equation (15)

$$G_{Cal} = \eta + 1.76 + L_R + T_1 + T_2 \tag{15}$$

where η is the antenna efficiency calculated using 10 $\log(R_D/ R_{in})$. $R_D = 0.079\ \Omega$ is obtained from the simulation results, while the wire conductivity is set to infinity. LR is

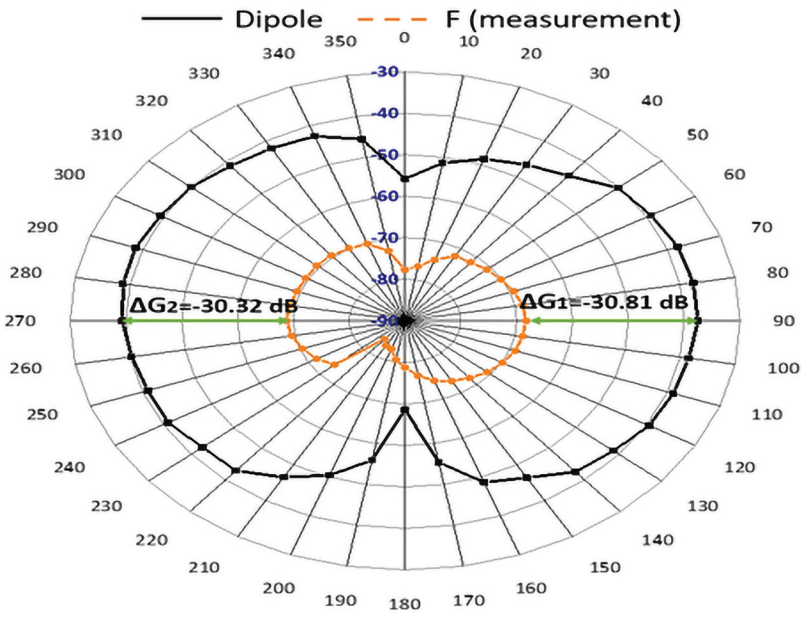

Figure 27. Measured radiation pattern of structure F and dipole antenna.

Table 5. Gain comparison of MLA in fat phantom.

$R_{in}(\Omega)$	LR(dB)	η(dB)	T1(dB)	T2(dB)	G_{Sim}(dBi)	G_{Cal}(dBi)	G_{Mea}(dBi)
48.95	−0.00054	−27	−1.59	−1.6	−30	−28.43	−28.42

the mismatch power loss, which is expressed by Equation (16)

$$L_R = 10\log\left(1 - \left(\frac{R_{in} - 50}{R_{in} + 50}\right)^2\right) \tag{16}$$

And T1 and T2 are the reflection coefficients from the vacuum (inside the phantom) to the phantom layer and the phantom layer to free space. They can be calculated by Equations (17) and (18), respectively.

$$T_1 = 10\log\frac{4n_1}{(n_1+1)^2} \tag{17}$$

$$T_2 = 10\log\frac{4n_2}{(n_2+1)^2} \tag{18}$$

For $T_1, n = \sqrt{\varepsilon_r}$and for $T_1, n = 1/\sqrt{\varepsilon_r}$. For fat tissue, $\epsilon_r = 12.21$ F/m. The calculated gain measured gain and simulated gain are compared in Table 5.

Regarding the gain comparisons in Table 5, G_{cal} is in agreement with the simulation value (G_{sim}). G_{meas} is also in agreement with G_{cal}. It is concluded that the antenna gain was confirmed through measurements.

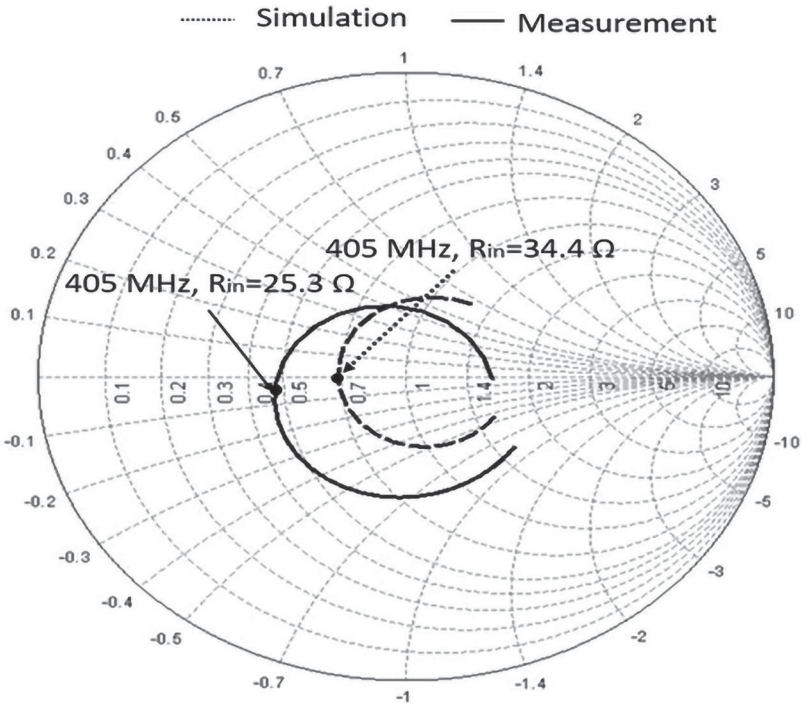

Figure 28. Input resistances of measured and simulated MLA in muscle tissue.

3.4. Measurement of input resistance of MLA in muscle

Input resistance at the resonant point of structure M with a dimension of 14.9 × 4.1 mm (L × W) and N = 6 was measured inside the fabricated phantom. The dielectric constant of the fabricated muscle phantom is $\epsilon_r = 56.1$ (F/m) and $\sigma = 0.71$ (S/m). The simulated and measured results of the input resistance (R_{in}) are presented in Figure 28. The solid curve is the measured result, while the dotted curve indicates the simulation result. From the simulation, the input resistance at 405 MHz is given as R_{in} (sim) = 34.3 **Ω**, while measured, it is obtained as R_{in} (meas) = 25.3 **Ω**. The measured results decreased from the simulation results by 9.1 **Ω**. However, this decrement might contribute to the effect of the feeding cable.

3.5. Antenna Q factor in muscle

The simulated and measured results of the VSWR are presented in Figure 24. The solid curve is the measured result, while the dotted curve indicates the simulation result. From the simulation, the frequency range at VSWR = 2 at 405 MHz is given as Δf (sim) = 306 MHz, while the measured value is obtained as Δf (meas) = 173 MHz.

The measured results decreased from the simulation results by 133 MHz. It is because of the impedance matching of the feeding cable of 50 Ω. The waveform and the frequency of the measurement result are slightly shifted to the right compared to the simulation

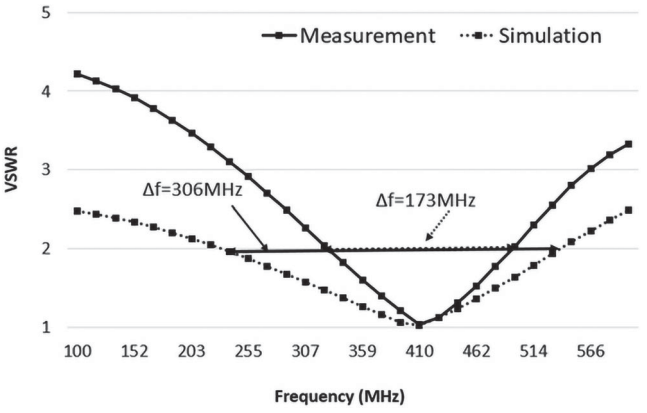

Figure 29. VSWR of measured and simulated MLA in muscle.

Table 6. Calculated values of Qeq and QVSWR.

Structure F	X_C (Ω)	R_{in} (Ω)	Δf (MHz)	Q_{eq}	Q_{VSWR}
Simulation	62.14	34.3	306	1.81	0.94
Measurement		25.3	173	2.45	1.65

results. The bandwidth of the simulation is 75.6 percent, and the measurement is 42.7 percent, respectively. As shown in Figure 29, the VSWR values of measurement results and simulation results of structure M have a good agreement.

Bandwidth (BW) can be calculated using Equation (8). The Q factor of VSWR can be obtained from Equation (9) [22]. The Q factor can also be calculated by the ratio of reactance to the input resistance (R_{in}) as expressed in Equation (10). The proposed inductive reactance (X_C) equation can be obtained by using Equation (11). Then Q factors obtained from X_C and VSWR can be compared as shown in Table 6.

According to Table 6, the Q factors obtained from Equations (10) and (11) are compared based on the simulation and measurement results. The simulation result of Q_{eq} is 1.81, and the simulation result of Q_{VSWR} is 0.94. The percent decrease is 48. In measurement, Q_{eq} is 2.45, and the Q_{VSWR} is 1.65. The percent decrease is 32. Moreover, simulation results and measured results of the Q factor have a good agreement. As a result, the simulation and equation results can be assumed to be consistent.

3.6. Measurement of antenna gain in muscle

The simulation results of three-dimensional (3D) radiation patterns of structure F are shown in Figure 30. The total realized gains of structure M are −40 dBi. The peak radiation direction appeared in the horizontal direction. The radiation pattern measurement comparisons of structure M to a half-wave dipole are shown in Figure 31.

In Figure 31, ΔG indicates the gain reduction of the half-wave dipole antenna. It means the gain difference between the MLA and the half-wavelength dipole. For structure M, ΔG1 and ΔG2 are −40.63 dB and −42.24 dB, respectively. The average ΔG is −41.435 dB. The calculated value of the antenna gain (Gcal) can be estimated using Equation (14).

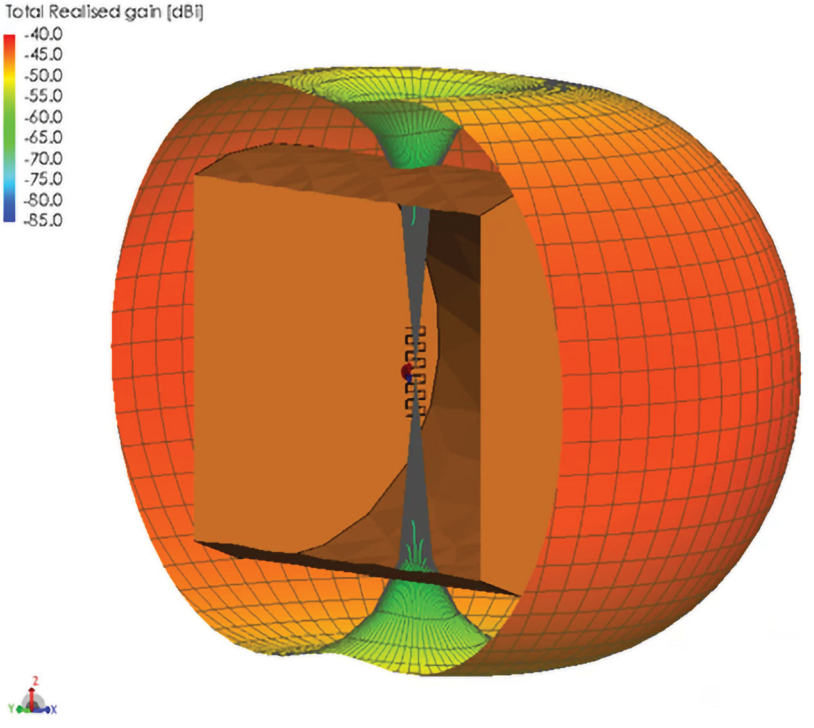

Figure 30. The three-dimensional radiation pattern of MLA in muscle.

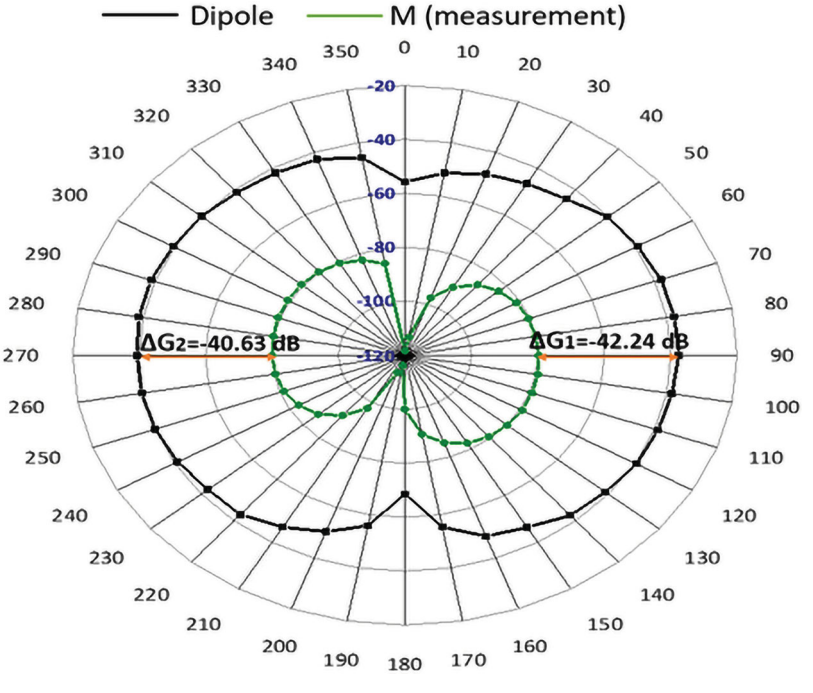

Figure 31. Measured radiation pattern of structure M and dipole antenna.

Table 7. Gain comparison of MLA in muscle phantom.

$R_{in}(\Omega)$	LR(dB)	η(dB)	T1(dB)	T2(dB)	G_{Sim}(dBi)	G_{Cal}(dBi)	G_{Mea}(dBi)
34.3	−0.15	−33.3	−3.84	−3.85	−40	−39.38	−39.28

Then, the measurement result of antenna gain can be calculated using Equation (13). The estimated gain can be obtained by using Equation (13), where η is the antenna efficiency calculated using $10\log(R_D/R_{in})$. $RD = 0.016\,\Omega$ is obtained from the simulation results, while the wire conductivity is set to infinity. The calculated gain, measured gain, and simulated gain are compared in Table 7. Regarding the gain comparisons in Table 7, Gcal agrees with the simulation value (Gsim). Gmeas is also in agreement with Gcal. It is concluded that the antenna gain was confirmed through measurements.

To illustrate this study's contribution, Table 8 compares the proposed MLA to various recently reported implanted antenna designs. As previously demonstrated, the majority of existing research has focused on planar or flexible implanted antennas that have been validated in free space, saline, or limited biological settings. While these designs have moderate bandwidth and small dimensions, they frequently lack rigorous phantom-based validation that simulates true human tissue properties. The suggested MLA has a reduced footprint ($14.9 \times 4.1 \times 0.1\,mm^3$), maintains a wide bandwidth (34–75%), and achieves acceptable gain values in fat and muscle phantoms.

4. Conclusion

In this study, an in-depth evaluation of the Meander Line Antenna (MLA) and its performance in muscle and fat tissue environments is presented, focusing on self-resonant conditions, radiation efficiency, and conductivity. The research highlights that the dielectric and conductive properties of muscle and fat significantly influence MLA performance. Muscle, with its high-water content and conductivity, presents challenges due to increased signal absorption and power loss, whereas fat, characterized by lower water content, offers comparatively higher radiation efficiency. By tailoring MLA configurations to align with the dielectric constants and conductivity of these tissues, the study identifies strategies for optimizing the antenna's efficiency and signal transmission within diverse biological contexts. Additionally, the analysis of input resistance and impedance matching underscores the importance of minimizing reflection losses and maximizing energy transfer. Exploring parameters such as Voltage Standing Wave Ratio (VSWR) and its relationship with the Q factor provides insights into improving the antenna's bandwidth and operational stability. These enhancements are crucial for ensuring reliable communication in implantable devices, supporting real-time monitoring and targeted therapeutic interventions.

Disclosure statement

No potential conflict of interest was reported by the author(s).

Table 8. Gain comparison of MLA in muscle phantom.

Reference	Antenna Type	Frequency (MHz)	Size (mm^3)	Bandwidth (%)	Gain (dBi)	Remarks
Malik et al. [2]	Planar implantable	402–405	20 × 10 × 1	∼ 25	−21	Validated in saline; no phantom fabrication
Kiourti et al. [5]	Miniaturized implant	915	12 × 12 × 0.5	30	−23	Optimized for ISM band; focus on flexible materials
Venkatachalam et al. [7]	Flexible planar	403	18 × 12 × 1	40	−25	Emphasized biocompatible substrate; limited validation
Hanna et al. [10]	Body-matched wearable	400–450	25 × 20 × 1	20	−28	Designed for glucose monitoring; external wearables
Baj-Rossi et al. [13]	Multi-panel implant	403	30 × 15 × 2	15	−26	Focused on metabolite monitoring system
This Work	Meander Line Antenna (MLA)	405	14.9 × 4.1 × 0.1	34–75 (meas.)	−30 (fat), −40 (muscle)	Systematic simulation + phantom measurement validation; strong agreement (∼ 92%)

References

[1] Jasim M, Al-Gburi AJA, Hanif M, et al. An extensive review on implantable antennas for biomedical applications: health considerations, geometries, fabrication techniques, and challenges. Alexandria Eng J. 2025;112:110–139. doi:10.1016/j.aej.2024.10.105

[2] Malik NA, Sant P, Ajmal T, et al. Implantable antennas for bio-medical applications. IEEE J Electromagn RF Microwaves Med Biol. 2020;5(1):84–96. doi:10.1109/jerm.2020.3026588

[3] Qing X, Chen ZN, See TSP, et al. Characterization of RF transmission in human body. In: 2010 IEEE Antennas and Propagation Society International Symposium. IEEE; 2010 Jul 11. p. 1–4. doi:10.1109/aps.2010.5561841.

[4] Yogev D, Goldberg T, Arami A, et al. Current state of the art and future directions for implantable sensors in medical technology: clinical needs and engineering challenges. APL Bioeng. 2023;7(3):031506. doi:10.1063/5.0152290.

[5] Kiourti A, Abbosh AM, Athanasiou M, et al. Next-generation healthcare: enabling technologies for emerging bioelectromagnetics applications. IEEE Open J Antennas Propag. 2022;3:363–390. doi:10.1109/ojap.2022.3162110

[6] Abd Rahman NH, Yamada Y, Amin Nordin MS. Analysis on the effects of the human body on the performance of electro-textile antennas for wearable monitoring and tracking application. Materials. 2019;12(10):1636. doi:10.3390/ma12101636

[7] Venkatachalam D, Jagadeesan V, Ismail KBM, et al. Compact flexible planar antennas for biomedical applications: insight into materials and systems design. Bioengineering. 2023;10(10):1137. doi:10.3390/bioengineering10101137

[8] Vallejo M, Recas J, Del Valle PG, et al. Accurate human tissue characterization for energy-efficient wireless on-body communications. Sensors. 2013;13(6):7546–7569. doi:10.3390/s130607546

[9] Shahid S, Wen P, Ahfock T. Effect of fat and muscle tissue conductivity on cortical currents-a tDCS study. In: The 2011 IEEE/ICME International Conference on Complex Medical Engineering. IEEE; 2011. p. 211–215. doi:10.1109/iccme.2011.5876735.

[10] Hanna J, Tawk Y, Azar S, et al. Wearable flexible body matched electromagnetic sensors for personalized non-invasive glucose monitoring. Sci Rep. 2022;12(1):14885. doi:10.1038/s41598-022-19251-z

[11] Dean D, Ramanathan T, Machado D, et al. Electrical impedance spectroscopy study of biological tissues. J Electrostat. 2008;66(3–4):165–177. doi:10.1016/j.elstat.2007.11.005

[12] Sowe M, Konditi DB, Langat PK. A compact high-gain microstrip patch antenna with improved bandwidth for 5G applications. Int J Electr Electron Res. 2022;10(2):196–201. doi:10.37391/ijeer.100225

[13] Baj-Rossi C, Kilinc EG, Ghoreishizadeh SS, et al. Full fabrication and packaging of an implantable multi-panel device for monitoring of metabolites in small animals. IEEE Trans Biomed Circ Syst. 2014;8(5):636–647. doi:10.1109/tbcas.2014.2359094

[14] Chou N, Moon H, Park J, et al. Interfacial and surface analysis of parylene C-modified PDMS substrates for soft bioelectronics. Prog Org Coat. 2021;157:106309. doi:10.1016/j.porgcoat.2021.106309

[15] Hlaing NW, Kamardin K, Yamada Y, et al. Analytical equations for designing meander line antennas. IEEE Open J Antennas Propag. 2024;5(2):340–353. doi:10.1109/OJAP.2023.3349145

[16] Shahpari M, Thiel DV. The impact of reduced conductivity on the performance of wire antennas. IEEE Trans Antennas Propag. 2015;63(11):4686–4692. doi:10.1109/tap.2015.2479241

[17] McCann H, Pisano G, Beltrachini L. Variation in reported human head tissue electrical conductivity values. Brain Topogr. 2019;32:825–858. doi:10.1007/s10548-019-00710-2

[18] Takiguchi M, Yamada Y. Radiation and ohmic resistances in very small meander line antennas of less than 0.1 wavelength. Electron Commun Jpn (Part I: Commun). 2005;88(8):1–11. doi:10.1002/ecja.20204

[19] Zainudin N, Abdul Latef T, Aridas NK, et al. Increase of input resistance of a normal-mode helical antenna (NMHA) in human body application. Sensors. 2020;20(4):958. doi:10.3390/s20040958

[20] Guido K, Matos C, Ramsey J, et al. Tissue-emulating phantoms for in vitro experimentation at radio frequencies: exploring characteristics, fabrication, and testing methods. IEEE Antennas Propag Mag. 2020;63(6):29–39. doi:10.1109/MAP.2020.3003208
[21] Nelson SO, Trabelsi S. Influence of water content on RF and microwave dielectric behavior of foods. J Microwave Power Electromagn Energy. 2008;43(2):13–23. doi:10.1080/08327823.2008.11688613
[22] Siragam S. Nanocomposite marvels: miniaturized high bandwidth microstrip patch antenna for X-band applications. Next Mater. 2024;5:100243. doi:10.1016/j.nxmate.2024.100243